Seamless Change Detection and Mosaicing for Aerial Imagery

Nimisha.T.M, A.N. Rajagopalan, R. Aravind
Indian Institute of Technology Madras
Chennai, India
{ee13d037,raju,aravind}@ee.iitm.ac.in

Abstract

The color appearance of an object can vary widely as a function of camera sensitivity and ambient illumination. In this paper, we discuss a methodology for seamless interfacing across imaging sensors and under varying illumination conditions for two very relevant problems in aerial imaging, namely, change detection and mosaicing. The proposed approach works by estimating surface reflectance which is an intrinsic property of the scene and is invariant to both camera and illumination. We advocate SIFT-based feature detection and matching in the reflectance domain followed by registration. We demonstrate that mosaicing and change detection when performed in the high-dimensional reflectance space yields better results as compared to operating in the 3-dimensional color space.

1. Introduction

With wide availability of imaging sensors, it has become common place to acquire images of a scene from different cameras and in different illumination conditions. This situation is, in fact, frequently encountered in aerial imaging wherein the reference and target images are typically captured at different times and not necessarily with the same camera. This can be either for surveillance purpose with unmanned aerial vehicles or for autonomous navigation and exploration. Algorithms that assume color change to arise from illumination alone will typically lead to erroneous results as they neglect the role of the camera in the entire process. In the literature, different methods have been developed for handling illumination variations including intensity normalization [1], albedo extraction [14], radiometric correction [12], white-balancing [4] to a canonical illumination and color correction [18].

A major drawback of these methods is the basic assumption of an infinitely narrow band spectral sensitivity which commercial cameras seldom satisfy. Also, these techniques assume that the images are acquired from the same camera which is a rather strong constraint. In [16] color change due to cameras is handled by finding a linear mapping between cameras or by finding two functions, one global and the other illumination-specific. These functions are learned for a pair of cameras; a RAW image of a scene can then be mapped from one camera to another. A drawback of this method is that each time a camera is changed, these functions need to be re-learned. Moreover, a linear mapping between cameras is valid provided (a) Luther's condition [17] is satisfied i.e. the camera sensitivity is a linear combination of human color responses, and (b) the reflectance lies in a lower-dimensional space. However, these assumptions hold only in limited cases.

Our goal in this work is to overcome the unwanted variabilities introduced by camera and illumination changes in change detection and mosaicing scenarios. Existing methods limit themselves to the same camera and mostly to the same illumination too. Variations, if any, unless accounted for, will show up as a false change or produce a visually unpleasant output. We allow for both camera and illumination changes by working in the reflectance domain. The color of an object we observe is the collective effect of our eyes' response, the object's surface spectral reflectance, and source illumination. By decomposing these components from the observed image, one can derive an illumination and camera invariant intrinsic property of the object; namely, the surface reflectance. Both change detection and mosaicing typically involve view-point changes too. For flat scenes, the observed images can be related by a homography. This, in turn, necessitates feature matching which clearly cannot be done in the RGB domain. We propose to perform registration using feature points detected and matched in the reflectance domain as it is invariant to both camera and illumination. We demonstrate that SIFT features [10] can be extracted and matched in the reflectance domain to compute the homography that relates the images. While change detection is carried out in the high-dimensional spectral domain by thresholding the reflectance difference (post-registration) at all spatial locations, mosaicing is performed at each wavelength and is then resynthesised specific to a given camera and illumination condition.

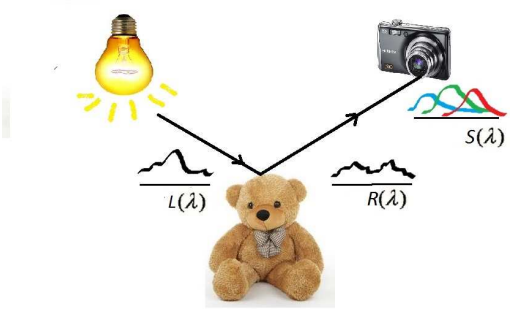

Figure 1. Image formation model.

The organization of this paper is as follows. Section 2 introduces the spectral image formation model. Section 3 discusses techniques to solve for the components in the image formation model. In Section 4, we propose registration in the spectral domain followed by methodologies for change detection and mosaicing. Section 5 contains experimental results while conclusions are given in Section 6.

2. Spectral image formation model

When light strikes an object, it is either absorbed or reflected depending on the material composition of the object. The reflected light is the color signal which is basically a product of the illumination spectrum and surface reflectance of the material. This color signal is filtered by the camera response function into three bands, typically Red, Green and Blue. Hence, the intensity value observed at a pixel position x is the cumulative effect of the camera, object spectral reflectance and illumination spectrum, and can be expressed as [16],

$$I_c(x) = \int_{\lambda \in V} R(x,\lambda) L(\lambda) S_c(\lambda) d\lambda \qquad (1)$$

where $c \in \{\text{R,G,B}\}$, V is the visible spectral range 400-700nm, $L(\lambda)$ is the illumination spectrum, $S_c(\lambda)$ is the camera spectral sensitivity, and $R(x,\lambda)$ is the surface spectral reflectance at position x. A pictorial representation depicting this relationship is shown in Fig. 1. Equation (1) is a special case of the dichromatic model proposed in [9].

The spectral reflectance $R(x,\lambda)$ can be interpreted as albedo image measured at a specific wavelength. This quantity is independent of the camera as well as scene illumination. The illumination spectrum $L(\lambda)$ depends on the temperature of the light source. It can be of different types with each type dominated by a particular wavelength or a wavelength interval. In this work, we discretize the visible spectrum (400-700nm) at intervals of 10nm as in [13]. Thus the spectrum of a light source is a 31-dimensional vector that spans the visible spectrum. In general, it is not possible to linearly relate two light sources having different illumination spectra, L_1 and L_2. Since only those wavelengths present in the light source that are not absorbed by the imaged object get reflected, different areas of the scene can get darkened or brightened differently depending upon the local reflectance. Hence, it is not possible, in general, to find a scalar α such that $L_1 = \alpha L_2$. The camera sensitivity $S_c(\lambda)$ is a set of three functions of wavelength specific to a camera that relates the color signal with the recorded RGB values. The effect of camera sensitivity on the acquired RGB image can be quite significant. Even under the same illumination, the images of a scene need not appear the same when viewed from different cameras as shown in Fig. 2. These images were taken with a Canon D600 and Nikon D5100 under tungsten lamp illumination with all other camera parameters (exposure time, aperture, ISO) fixed. The color change in Fig. 2 is caused by difference in the camera sensitivity alone.

(a) (b)

Figure 2. Color changes due to difference in camera sensitivity. (a) Image taken with Canon D600 under tungsten lamp illumination. (b) Image taken with Nikon D5100 under the same illumination.

3. S/L/R Estimation

The acquired RGB color image is the cumulative effect of camera, illumination and scene reflectance. To estimate each of these components independently given only the RGB data is quite an ill-posed problem.

Camera sensitivity is usually measured with a monochromator and spectrophotometer [11], which can be time-consuming. In [8], camera sensitivity is estimated from a single image by assuming that it is spatially-invariant and non-negative. The authors determine a low-dimensional statistical model for the whole space of camera sensitivity and learn the basis functions for this space such that any camera sensitivity can be estimated for known and unknown illumination conditions from a single image. They have provided a database containing the sensitivity of 28 different cameras in [1]. We too used this spectral sensitivity data in our experiments.

The illumination spectrum mainly depends on the temperature of the light source. There are works [2] that estimate illumination using color from correlation. They estimate the likelihood of each possible illuminant from the observed data. Other techniques for illumination estimation

[1] http://www.cis.rit.edu/jwgu/research/camspec/db.php

include grey world algorithms which assume the average surface reflectance to be stable and any difference from the stable point is attributed to illumination variation.

Surface reflectance is the intrinsic property of a scene and provides a camera and illuminant-independent domain to work with. Although the spectral information can be captured directly by using hyperspectral cameras, this is prohibitively expensive. Many works have discussed retrieving spectral data from commercial cameras [6], [7]. PCA-based methods for spectral reflectance estimation [6] assume reflectance to be from a lower-dimensional space and learn the basis functions of this space. Other techniques are based on multiple images acquired with specialized filters or a Digital Light Processing (DLP) projector [5] etc. But these require additional hardware.

We discuss here a method [13] that jointly solves for both illumination (L) and reflectance (R), given the color image.

$$I = S.\text{diag}(L).R_l \tag{2}$$

$R_{l(k\times MN)}$ is the vectorized form of R whose row represents the albedo image estimated at a particular wavelength. Assuming the knowledge of the camera sensitivity ($S_{3\times k}$) discretized by sampling the interval from 400-700 nm and given the RGB value ($I_{M\times N}$) at each pixel position in the image, solving the above equation for illumination spectrum ($L_{1\times k}$) and reflectance spectrum ($R_{M\times N\times k}$) is quite challenging. There are basically $3MN$ knowns from which we need to solve for $k(MN$+1) unknowns where k = 31. In the training phase of [13] , a set of hyperspectral data is collected wherein the scene contains a white tile. The illuminant spectrum is separated from the imaged white tile by averaging the spectral response of white tile pixels over the captured range of spectrum. Once the illuminant is found out, the reflectance is calculated from the hyperspectral data by dividing it with the illuminant spectrum. With the RGB images and ground truth reflectance in hand, training is done to learn a mapping from the 3-dimensional RGB value to the high-dimensional reflectance value using radial basis functions (RBF). Along with this mapping, a PCA-based basis function for illumination is also learnt. Once training is over, a reflectance and illumination model specific to the camera is generated. Any RGB image taken with this specific camera can now be decomposed into its reflectance and illuminant spectra using the model thus learned. Note that since the mapping function is nonlinear, a linear variation in the RGB domain will not be reflected as a linear change in the reflectance domain. Also, since illumination and reflectance spectra are estimated together, error in one can propagate into the other.

4. Change Detection and Mosaicing

As discussed in the beginning, the goal of this paper is to enable change detection and mosaicing, irrespective of camera and illumination considerations.

Change detection involves estimating the change map between two images $I^{(1)}$ and $I^{(2)}$ of a scene taken with different cameras and illumination along with view-changes (if any). Let $R(x,\lambda)$, $L^{(1)}(\lambda)$ and $S^{(1)}(\lambda)$ be the scene reflectance, illumination spectrum and camera sensitivity, respectively. Then, image $I^{(1)}$ can be expressed as

$$I_c^{(1)}(x) = \int R(x,\lambda)L^{(1)}(\lambda)S_c^{(1)}(\lambda)d\lambda$$

Let $I^{(2)}$ be the second image taken at a different time and with a different camera. It is given by

$$I_c^{(2)}(x') = \begin{cases} \int R(\tau(x),\lambda)L^{(2)}(\lambda)S_c^{(2)}(\lambda)d\lambda, & \text{if } x' \notin \mathcal{C} \\ \int R_o(x',\lambda)L^{(2)}(\lambda)S_c^{(2)}(\lambda)d\lambda, & \text{if } x' \subseteq \mathcal{C} \end{cases} \tag{3}$$

where τ represents geometric warping due to view-change, $\mathcal{C}$ is the set of occluding pixel positions in the image, and R_o is the spectral reflectance of the occluding object. Note that the reflectance from $I^{(2)}$ could be either from the occluding object's reflectance or from the geometrically warped reflectance of the original image. The geometric changes in the original image are directly mapped onto the reflectance domain. The problem of change detection thus boils down to finding the occluder (when present).

As a first step, the reference and target images need to be registered. SIFT [10] is a popular feature detector that has been widely used in monochromatic images. Since the acquired RGB image depends on the camera and illumination, the extracted SIFT features are not consistent. Hence, we propose feature matching and registration in the reflectance domain. The SIFT features can be reliably detected since reflectance is an intrinsic property. The features are then matched across the two reflectance images. Once the correspondences are found, Random sample consensus (RANSAC) [3] is used to estimate the homography matrix relating the geometric variation between the two images. To address the issue of choice of the best band, we considered wavelengths corresponding to the maximum of *Commission Internationale de L'Eclairage* (CIE) standard observer color matching functions (i.e. 450, 550 and 600 nm approximately) and convert this to a grayscale image for SIFT feature calculation. Fig. 3 shows feature matches across two reflectance images, where the second image is a translated and occluded version of the first. Only the first few correspondences are shown in the figure.

Using the estimated homography, the reflectance images at all wavelengths are registered. Then, a reflectance image stack is formed where each pixel location in the spatial domain is associated with a 31×1 spectral data along the wavelength axis. Since the reflectance data is material-specific and changes with the material composition of the object, it gives more information about the acquired image

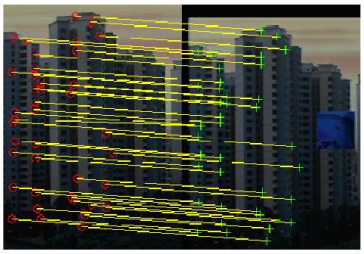

Figure 3. Matched features in reflectance images.

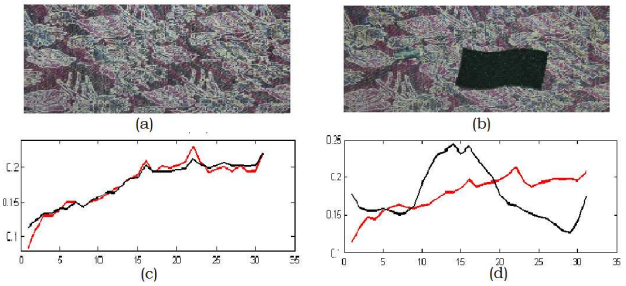

Figure 4. Variation of reflectance spectra. (a) Image 1. (b) Image 2 with occlusion. (c) The reflectance spectra at a non-occluding pixel position. (d) Reflectance spectra corresponding to an occluding pixel.

at each spatial location as compared to using the RGB image which is a filtered and dimensionality reduced version of this high-dimensional spectral data.

As shown next, the spectral information can be effectively used for performing change detection. Figs. 4(a) and 4(b) represent two images of the same scene taken with Canon 60D under fluorescent lighting. Subplot (c) shows the surface reflectance at a non-occluding pixel position whereas (d) shows the reflectance corresponding to an occluding pixel position. Note that the introduction of a new object into the scene changes the surface reflectance information at those pixel positions. By thresholding the Euclidean distance between the surface reflectance data at each spatial location in the reference and target images, one can arrive at the change map.

The goal in image stitching is to produce a panorama corresponding to any single camera and arbitrary illumination. Let there be a total of n images $(I^{(i)}; i = 1, 2..., n)$ captured under n different light conditions $(L^{(i)}, i = 1, 2.., n)$ and cameras with sensitivities $(S^{(i)}, i = 1, 2, .., n)$ i.e.

$$I_c^{(i)}(x') = \begin{cases} \int R(\tau_{ij}(x), \lambda) L^{(i)}(\lambda) S_c^{(i)}(\lambda) d\lambda, & \text{if } x' \subseteq \mathcal{M}_{ij} \\ \int R_i(x', \lambda) L^{(i)}(\lambda) S_c^{(i)}(\lambda) d\lambda, & \text{if } x' \nsubseteq \mathcal{M}_{ij}, \end{cases} \quad (4)$$

where $\mathcal{M}_{ij}$ is the set of overlapping pixel positions in $I^{(i)}$ and $I^{(j)}$ $(i \neq j)$ and R_i is the reflectance of the non-overlapping new information captured in scene $I^{(i)}$. In the overlapping regions, $I^{(i)}$ is related to $I^{(j)}$ by a warping τ_{ij}, and camera, and illumination changes. The reflectance images are warped versions of each other and are independent of camera or illumination. The non-overlapping regions in $I^{(i)}$ bring in new information. The reflectance images are registered using a similar approach as discussed earlier under change detection. Mosaicing is carried out in the reflectance domain to overcome undesirable artifacts caused by color changes. Let R_s represent the stitched reflectance image. Then the mosaiced RGB image $(M^{(i)})$ as seen from the i^{th} camera can be synthesized as

$$M_c^{(i)}(x) = \int R_s(x, \lambda) L(\lambda) S_c^{(i)}(\lambda) d\lambda \quad (5)$$

The stitched reflectance image can also be relighted with a specific illumination $(L^{(i)})$ as

$$M_c^{(i)}(x) = \int R_s(x, \lambda) L^{(i)}(\lambda) S_c(\lambda) d\lambda \quad (6)$$

5. Experimental results

For evaluating the performance of the proposed framework, we test on both synthetic and real examples. Along with qualitative and quantitative assessment, we also provide comparisons. In order to acquire images from different cameras and illumination, we used the hyperspectral dataset given in [13]. RGB images are synthesized by multiplying the spectral data with each camera's sensitivity provided in the database of [8]. For the synthetic experiments, we considered four cameras: Canon 600D, Canon 1D Mark III, Nikon D40 and Olympus E PL2. Real examples were captured with Canon 60D, Nikon D5100 and Fujifilm S4800 cameras, for which the sensitivities are available in the database. The light sources used for illumination are sunlight and metal halide lamp at different temperatures: 2500K, 3000K, 4500K and 6500K. Once the RGB images are synthesized, the reflectance is estimated using the learned camera-specific RBF [13] discussed in Section 3. All our results are displayed in color.

Change detection:

There are different ways in which two images can be compared. We discuss relevant situations below and compare our output with each one of these.

1. Variant 1: Image registration, pixel-wise subtraction and thresholding, all in the RGB domain, without any photometric corrections.

2. Variant 2: Accommodating for color changes by using color-transfer algorithms and transferring color of target image to source image. This is followed by registration, pixel-wise subtraction and thresholding of the color-corrected images.

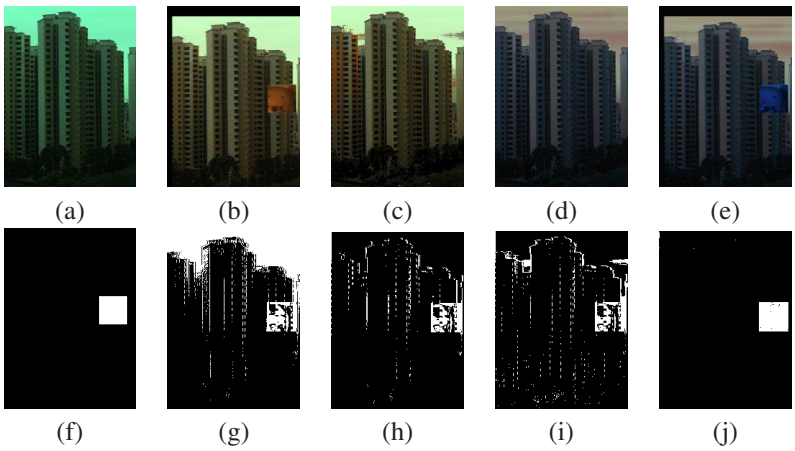

Figure 5. Synthetic experiment on change detection. (a) Input image 1. (b) Input image 2 with occlusion and view-change. (c) Color of image 2 transferred to that of image 1. (d, e) Reflectance images estimated from image 1 and image 2. (f) Ground truth change map. (g) Change map using RGB image (PCC = .8089, JC = .1154, YC = .1066). (h) Change map obtained from white-balanced image (PCC = .9617, JC = .3803, YC = .4798). (i) Change map using color-transferred image (PCC = .9476, JC = .2946, YC = .3574). (j) Our result (PCC = **.9997** , JC = **.9923**, YC = **.9985**).

Figure 6. Synthetic example on change detection. (a, b) Synthesized source and target images. (c) Color transferred image. (d, e) Reflectance images derived from image 1 and image 2 at wavelengths (450,550 and 600 nm). (f) Ground truth occlusion. (g) Output of change detection directly in RGB domain (PCC = .5818, JC = .0264, YC = .0260). (h) White-balanced change detection (PCC = .8260, JC = .0611, YC = .0610). (i) Color-transferred change detection (PCC = **.9987**, JC = **.8950**, YC = .9192). (j) Change map using our method (PCC = .9986, JC = .8699, YC = **.9933**).

3. Variant 3: White-balancing the images and then performing registration, pixel-wise differencing and thresholding of the white-balanced images.

The first image in Fig. 5 is synthesized from the hyperspectral data in [13] as seen from a Canon 1D Mark III camera under daylight illumination. The second image is simulated with view-change, occlusion and as observed from Olympus E PL2 camera but under same illumination. The reflectance and illumination spectra are estimated from both the input images. From the reflectance images, the wavelengths corresponding to maxima in CIE are chosen to form a color image which is converted to gray format for feature detection. We used vlfeat toolbox [19] for detecting and matching SIFT features. In the second synthetic example (Fig. 6), the first image is synthesized with Canon 1D Mark III camera under Metal halide lamp 6500K whereas the second image is synthesized with occlusion and view-change as seen from Canon 600D under Metal halide 2500K.

The results corresponding to our method as well comparisons with variants 1, 2 and 3 are given in Figs. 5 and 6. Note that the RGB input images in the synthetic experiments shown in Figs. 5(a) and (b) and Figs. 6(a) and (b), synthesized with different cameras and illumination, show significant color variations which leads to error in the estimated change map in Figs. 5(g) and 6(g). The color transferred images in Figs. 5(c) and 6(c) were produced by using the code provided by the authors of [15]. The errors caused by improper color transfer show up as false changes in the final output (Figs. 5(i) and 6(i)). The error in Fig. 6(i) is somewhat less with small grains in the color transferred out-

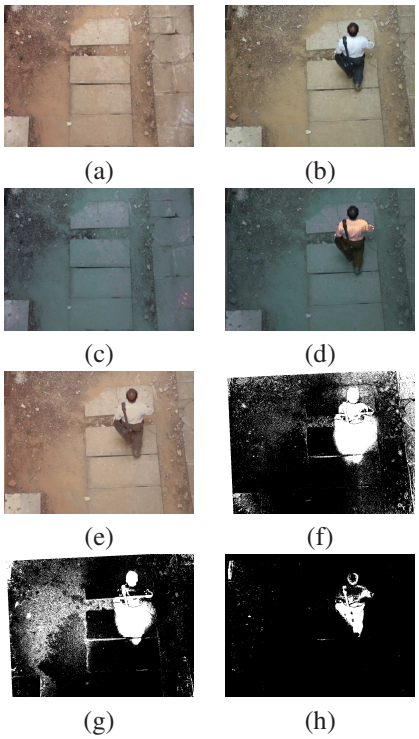

Figure 7. Change detection on a real dataset. (a, b) Reference and target images captured with Fujifilm and Canon 60D, respectively. (c, d) Reflectance images estimated from the inputs at wavelengths 450, 550 and 600 nm. (e) Color of reference image mapped to target image. (f) Changes detected directly from the captured RGB images. (g) Change detected post color transfer. (h) Output of the proposed method.

put showing up as change. Figs. 5(h) and 6(h) are change maps obtained after white-balancing the input RGB images. Though white-balancing removes illumination variations to some extent, the variations caused by camera sensitivity are not corrected which show up as error in the change map. In contrast, the result of our method given in Figs. 5(j) and 6(j) produces a change map that is visually closest to to the ground truth.

We also performed quantitative evaluation based on the following well-known metrics for change detection.

1. Percentage of correct classification PCC $= \frac{TP+TN}{TP+TN+FP+FN}$.
2. Jaccard coefficient JC $= \frac{TP}{TP+FP+FN}$
3. Yule coefficient YC $= |\frac{TP}{TP+FP} + \frac{TN}{TN+FN} - 1|$

Here TP represents the number of changed pixels correctly detected, FP represents number of no change pixels marked as changed, TN is the number of no change pixels correctly detected, and FN is number of change pixels incorrectly labeled as no change. PCC alone can give

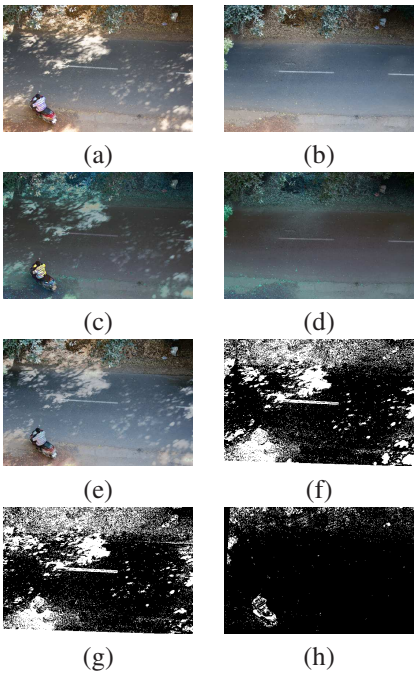

Figure 8. Real experiment on change detection with both camera and illumination changes. (a) Image taken with Canon 60D camera. (b) Image taken with Nikon D5100. (c) and (d) are the estimated reflectance images. (e) Color-transferred image from (b) to (a). (f) Changes detected in the RGB domain. (g) Changes detected after color-transfer. (h) Changes detected using our method.

misleading results when the size of the occluder is small compared to the overall image. JC and YC overcome this issue by minimizing the effect of the expected large volume of TN. These coefficients should be close to 1 for an ideal case. However, in practice, a value greater than 0.5 is considered quite good for JC and YC. Values of PCC, JC and YC are given in the captions of Figs. 5 and 6 for each method. From these values, it is clear that even though other methods show comparable PCC values, they fail to yield good numbers for YC and JC. In contrast, our method consistently delivers good values for all the coefficients.

Results on change detection for real images are given in Figs. 7 and 8. The first image in Fig. 7 is taken using a Fujifilm S4800 camera whereas the second image is taken with Canon 60D. Both these images are taken under same daylight illumination. The color difference caused by camera change is clearly visible in these images. In Fig. 8, the first and second image are taken with Canon 60D and Nikon D5100, respectively, and at different times. Note the change in illumination in the two images. From the outputs shown in Figs. 7(f)-(h) and 8(f)-(h), it is clear that our algorithm outperforms competing methods even in challenging real scenarios. Although there are artifacts in our output, these are very few as compared to other

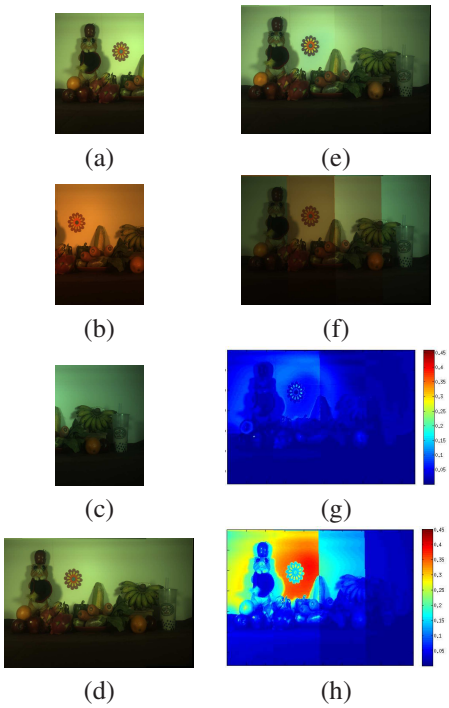

Figure 9. (a-c) are input images for stitching. (d) Ground truth panorama. (e) Resynthesized stitched image using our method and as seen with Canon 1D Mark III camera under Metal Halide 3000K (RMSE = **0.0431**, SSIM = **0.9595**). (f) Stitched image in RGB domain (RMSE = 0.1325, SSIM = 0.7890). (g) Error map between (d) and (e). (h) Error map between (d) and (f).

methods.

Image Mosaicing:

For synthetic experiments, we divided the hyperspectral data [13] of a scene (across all wavelengths), into three spatially overlapping regions. The RGB images corresponding to these three regions are synthesized as observed from Canon 1D Mark III, Nikon D40 and Canon 600D cameras and under Metal Halide 3000K, Metal Halide 2500K and daylight illumination, respectively. Thus, we obtained the three input images shown in Figs. 9(a)-(c). The images together cover a wider field of view. We estimated the reflectance and illumination spectra from these input images. We also account for translation motion in this example. The homography matrices relating these reflectance images are estimated using SIFT features and the reflectance images are stitched in all the wavelengths. The stitched reflectance image is transformed into an RGB image as seen from Canon 1D Mark III under Metal Halide 3000K as shown in Fig. 9(e). The result of stitching directly in the RGB domain is given in Fig. 9(f). The ground truth image of this scene (Fig. 9(d)) is produced by directly combining the spectral reflectance data provided in the dataset [13] with

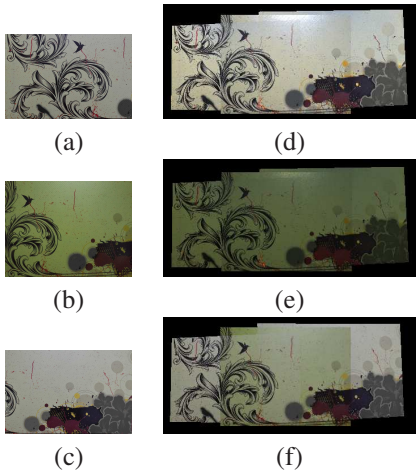

Figure 10. Real experiment for an indoor scene. (a) and (c) are input images taken with Nikon D5100. (b) Input image taken with Fujifilm (all the images were taken under fluorescent lighting). (d) and (e) Mosaiced output of our method as viewed under Nikon D5100 and Fujifilm. (f) Image stitched directly in the RGB domain.

the specified illumination and camera sensitivity. The error maps with respect to the ground truth image are given in Figs. 9(g) and (h). Quantitative analysis with respect to ground truth image is given in terms of RMSE and SSIM in the caption of Fig. 9.

Finally, we give results on real mosaicing examples. Figs. 10(a)-(c) show input images taken with Nikon D5100 and Fujifilm S4800 in indoor settings with fluorescent illumination. The stitched image in the reflectance domain is then resynthesized as seen from these cameras. Figs. 11(a)-(c) represent input images of an outdoor scene taken with Canon 60D and Fujifilm S4800 and under daylight illumination. From the stitched output images in Figs. 10(d)-(f) and Figs. 11(d)-(f), we can observe that the results of the our proposed method look visually pleasing.

6. Conclusions

In this paper, we discussed an important effort aimed at achieving inconspicuous change detection and mosaicing across different cameras and illumination variations. We showed that color variations caused by changes in camera and illumination can be robustly handled to a good extent by working in the reflectance domain. We also demonstrated that feature extraction and registration can be done efficiently in the reflectance domain due to its invariant characteristics. Synthetic as well as real examples on change detection and mosaicing were given to validate the proposed framework.

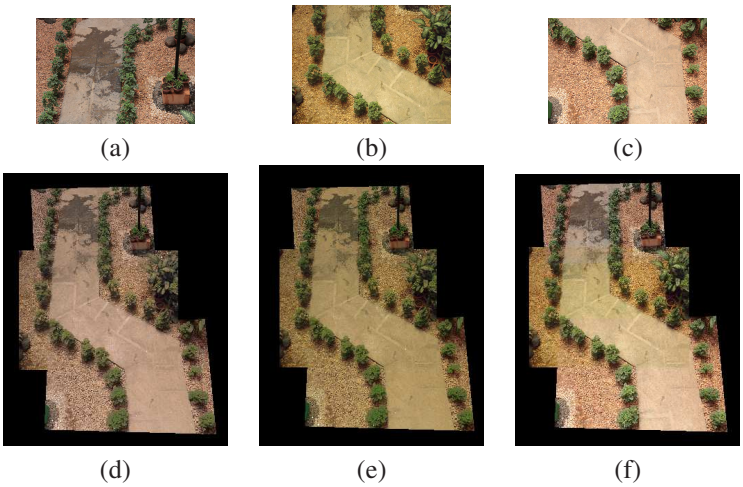

Figure 11. Mosaicing of an outdoor scene. (a) and (c) are images taken with Canon 60D. (b) Image taken with Fujifilm. (d) Stitched image in the reflectance domain and resynthesized as seen from Canon 60D camera using our method. (e) Stitched image in the reflectance domain and resynthesized as seen from the Fujifilm camera using our method. (f) Image stitched directly in the RGB domain.

References

[1] X. Dai and S. Khorram. The effects of image misregistration on the accuracy of remotely sensed change detection, 1998. IEEE Trans. Geoscience and Remote Sensing. 1

[2] G. D. Finlayson, S. D. Hordley, and P. M. Hubel. Colour by correlation: A simple, unifying approach to colour constancy. In *Computer Vision, 1999. The Proceedings of the Seventh IEEE International Conference on*, volume 2, pages 835–842. IEEE, 1999. 2

[3] M. A. Fischler and R. C. Bolles. Random sample consensus: a paradigm for model fitting with applications to image analysis and automated cartography. *Communications of the ACM*, 24(6):381–395, 1981. 3

[4] A. Gijsenij, Gevers, and J. van de Weijer. Computational color constancy: Survey and experiments. *Image Processing, IEEE Transactions on*, 20(9):2475–2489, 2011. 1

[5] S. Han, I. Sato, T. Okabe, and Y. Sato. Fast spectral reflectance recovery using dlp projector. *International Journal of Computer Vision*, 110(2):172–184, 2014. 3

[6] V. Heikkinen, R. Lenz, T. Jetsu, J. Parkkinen, M. Hauta-Kasari, and T. Jääskeläinen. Evaluation and unification of some methods for estimating reflectance spectra from rgb images. *JOSA A*, 25(10):2444–2458, 2008. 3

[7] J. Jiang and J. Gu. Recovering spectral reflectance under commonly available lighting conditions. In *Computer Vision and Pattern Recognition Workshops (CVPRW), 2012 IEEE Computer Society Conference on*, pages 1–8. IEEE, 2012. 3

[8] J. Jiang, D. Liu, J. Gu, and S. Susstrunk. What is the space of spectral sensitivity functions for digital color cameras? In *Applications of Computer Vision (WACV), 2013 IEEE Workshop on*, pages 168–179. IEEE, 2013. 2, 4

[9] G. J. Klinker, S. A. Shafer, and T. Kanade. A physical approach to color image understanding. *International Journal of Computer Vision*, 4(1):7–38, 1990. 2

[10] D. G. Lowe. Object recognition from local scale-invariant features. In *Computer vision, 1999. The proceedings of the seventh IEEE international conference on*, volume 2, pages 1150–1157. Ieee, 1999. 1, 3

[11] J. Nakamura. *Image sensors and signal processing for digital still cameras*. CRC press, 2005. 2

[12] S. Negahdaripour. Revised definition of optical flow: integration of radiometric and geometric cues for dynamic scene analysis. *IEEE Trans. Pattern Anal. Machine Intell.*, 20(9):961–979, 1998. 1

[13] R. M. H. Nguyen, D. K. Prasad, and M. S. Brown. Training-based spectral reconstruction from a single rgb image. *ECCV*, 7(11):186–201, 2014. 2, 3, 4, 5, 7

[14] B. Phong. Illumination for computer generated pictures, 1975. Commun. ACM. 1

[15] F. Pitié, A. C. Kokaram, and R. Dahyot. Automated colour grading using colour distribution transfer. *Computer Vision and Image Understanding*, 107(1):123–137, 2007. 5

[16] N. H. M. Rang, D. K. Prasad, and M. S. Brown. Raw-to-raw: Mapping between image sensor color responses. In *2014 IEEE Conference on Computer Vision and Pattern Recognition, CVPR 2014, Columbus, OH, USA, June 23-28, 2014*, pages 3398–3405, 2014. 1, 2

[17] J. C. Seymour. Why do color transforms work? In *Electronic Imaging'97*, pages 156–164. International Society for Optics and Photonics, 1997. 1

[18] Thomas, K. Bowyer, and A. Kareem. Color balancing for change detection in multitemporal images. *Applications of Computer Vision (WACV)*, 9(11):385–390, 2012. 1

[19] A. Vedaldi and B. Fulkerson. VLFeat: An open and portable library of computer vision algorithms. http://www.vlfeat.org/, 2008. 5